Applied Surface Science 576 (2022) 151768

Contents lists available at ScienceDirect

Applied Surface Science

journal homepage: www.elsevier.com/locate/apsusc

Full Length Article

Inhibition of biofilm formation induced by functional graphenic materials impregnated in Nile tilapia (Oreochromis niloticus) skin

Fernando Antonio Gomes da Silva Jr. [a], Karoline E. Eckhart [b], Mateus Matiuzzi da Costa [a], Stefanie A. Sydlik [b], Helinando Pequeno de Oliveira [a,*]

[a] Institute of Materials Science, Federal University of São Francisco Valley, Avenida Antônio Carlos Magalhães, 510 - Santo Antônio, CEP: 48902-300 – Juazeiro, BA, Brazil

[b] Department of Chemistry, Carnegie Mellon University, Pittsburgh, PA 15213, USA

ARTICLE INFO

Keywords:
Graphenic materials
Xenograft
Tilapia skin
Biofilm
Bacteria

ABSTRACT

Wound dressings based on natural materials, such as fish skin, represent an important strategy for the treatment of burns. Despite their utility, contamination of these natural materials with bacteria (planktonic and biofilm forms) introduces significant risks to patients under treatment. This disadvantage can be overcome by modifying the material's surface to prevent bacterial deposition through chemical or physical interactions. In this work, functional graphenic materials (FGM) with tunable surface charges were incorporated into tilapia (*Oreochromis niloticus*) fish skin as a part of a strategy to control the biofilm adhesion on surfaces. The antibiofilm activity was evaluated against *S. aureus* and *K. pneumoniae* due to the biofilm-forming properties of these bacterial strains. FGM-modified tilapia skin samples possess a strong capacity to reduce biofilm formation on the tilapia fish skin with a higher antibiofilm activity against Gram-positive bacteria, compared to Gram-negative bacteria. Negatively charged FGMs were more effective than positively charged FGMs in preventing biofilm formation on the impregnated tilapia skin xenografts: negatively charged Claisen graphene achieved an 88.8% reduction in biofilm formation on the tilapia skin. Overall, this study demonstrates the utility of FGM-impregnated tilapia skins as a treatment for burn wounds due to their ability to modulate bacterial adhesion.

1. Introduction

Globally, burns are responsible for 180,000 annual deaths; and bacterial infection ranks as one of the leading causes of burn patient death [1-3]. Bacterial infection can significantly delay wound healing, detract from patient quality of life, and increase treatment costs [4,5]. Because of this, there is considerable interest in enhancing the therapeutic effects of traditional burn wound dressings to enable more rapid and safer healing and to prevent bacterial infection [5]. Several strategies have been employed to provide antimicrobial protection and accelerated healing of skin wounds and burns. These include silver-based formulations [6,7], hyperbaric oxygen therapy, negative pressure wound therapy, cell therapy [8], and biological-based treatments such as allografts, xenografts, and bioengineered modified tissues [6].

Scaffolds made with natural materials, such as biopolymers and biological tissue, have versatile mechanical, physical, and biological properties that are advantageous in wound dressing applications [9]. These scaffolds exhibit favorable characteristics including good biocompatibility, coupled with non-irritating and non-toxic properties [10]. Scaffolds with high collagen content introduce beneficial properties including low antigenicity, increased hemostasis, and accelerated fibroplasia and epithelialization [6].

The use of Nile tilapia skin for the treatment of burns and wounds introduces advantages due to its abundance, mechanical match to human skin, and chemical composition that supports wound healing. Nile tilapia (*Oreochromis niloticus*) is an abundant resource found in tropical and subtropical regions; it is the most commonly cultivated fish in Brazil and ranks fourth in the world, according to the United Nations Food and Agriculture Organization [7]. Tilapia skin offers good mechanical compatibility with human skin, and high strength and extension before rupture [1,6,11], making it a suitable xenograft material for wound treatment [1,2,12,13]. Further, marine fish skin contains chemical components such as collagen peptides, polyunsaturated and omega-3 fatty acids, polyunsaturated fatty acids, eicosapentaenoic acid,

Abbreviations: FGM, functional graphenic material; TS, tilapia skin; GO, graphene oxide; CG, Claisen graphene; PLL-G, poly-L-lysine-graphene conjugate.

* Corresponding author.
E-mail address: helinando.oliveira@univasf.edu.br (H. Pequeno de Oliveira).

https://doi.org/10.1016/j.apsusc.2021.151768
Received 24 August 2021; Received in revised form 18 October 2021; Accepted 28 October 2021
Available online 6 November 2021

and docosahexaenoic acid that have been shown to support healing [14,15]. Due to these advantageous properties, tilapia skin has been used in several biomedical applications, such as an occlusive burn dressing [1], metacarpal wound dressing [16], and as a xenograft in gynecology for the treatment of Mayer-Rokitansky-Küster-Hauser syndrome [17].

Tilapia skin offers several benefits over mammalian-sourced skin. Although mammalian skin exhibits favorable mechanical and chemical properties that support its utility in wound dressing applications, biological dressings based on mammalian skin carry a risk of disease transmission and their use is discouraged in some religions and cultures [18]. On the other hand, marine fish skin carries less of a risk of disease transmission, compared to mammalian-sourced skin, and does not have ethical and culture barriers [14]. Further, unlike mammalian skin grafts which require chemical sterilization with toxic ethylene oxide gas (which reacts for form hazardous products that pose a potential risk to the patient) [19,20], tilapia skin specimens only require a gentle sterilization method involving chemical sterilization with a mild antiseptic, glycerolization, and irradiation [2]. Depending on the method of sterilization, fish skin may still contain residual microorganisms derived from their aquatic environment or other sources of contamination [6].

Antibiotics are commonly administered in conjunction with xenografts to prevent pathogenic bacteria from creating a biofilm on the xenograft [21]. Biofilm formation is a significant risk in xenografts because they serve as an excellent, albeit nonspecific, platform for cellular adhesion [15]. Once a biofilm is established, it is notoriously difficult to eradicate: bacteria in a biofilm have higher resistance to traditional antibiotics and are protected from host immune defenses by their dense extracellular matrix [22]. Bacterial contamination and subsequent biofilm formation on xenograft implants can be suppressed using conventional antibiotics. For example, antibiotic clindamycin has been incorporated into bone xenograft composites to eradicate *Staphylococcus aureus (S. aureus)* contamination during bone regeneration in vivo [23]. Additionally, porcine skin xenografts have been decontaminated by washing with various antibiotics (streptomycin, chloramphenicol, and nitrofurantoin), resulting in a reduction of planktonic *S. aureus*; although, as expected, biofilm bacteria were significantly less susceptible to antibiotic washing [24]. Further, wound dressings impregnated with an antibiotic have been shown to prevent the colonization of *S. aureus* in burn wounds and reduce pathogenic activity that varies from endocarditis to septicemia [25]. Notably, repeated use of conventional antibiotics can cause bacteria to develop resistance mechanisms [26]. This risk of antibiotic resistance highlights the critical need to explore alternative strategies to suppress bacterial growth on xenograft substrates without the use of conventional antibiotics.

Previous works published by our groups have demonstrated that electrostatic interaction between charged surfaces and bacteria can be leveraged to prevent bacterial adhesion processes, thus reinforcing the overall antibacterial activity of the system. Specifically, positively charged polypyrrole [27-30] and polyaniline [31] have been explored as antibacterial supports that interact with negatively charged bacterial membranes to inhibit bacterial growth on surfaces. Additionally, functional graphenic materials (FGMs) [32] with tunable surface charge were used as bacterio-instructive scaffolds for controlling the degree of bacterial adhesion on the FGM surface. These FGMs have the added advantage of being biocompatible materials with lower toxicity than typically observed for conductive polymers [32].

Herein, FGMs with various surface charges were incorporated into tilapia skin as a part of a strategy to avoid the biofilm formation of *S. aureus* and *K. pneumoniae* and to improve the resulting properties of the modified skin as a prototype for wound dressing applications. In this work, disks of tilapia fish skin were doped with negatively and positively charged FGMs, imparting antibiofilm properties to the tilapia skin surface (Fig. 1). These FGM-impregnated tilapia fish skins provide a biofilm-protective barrier that addresses the critical need to prevent burn wound infection without the use of traditional antibiotics.

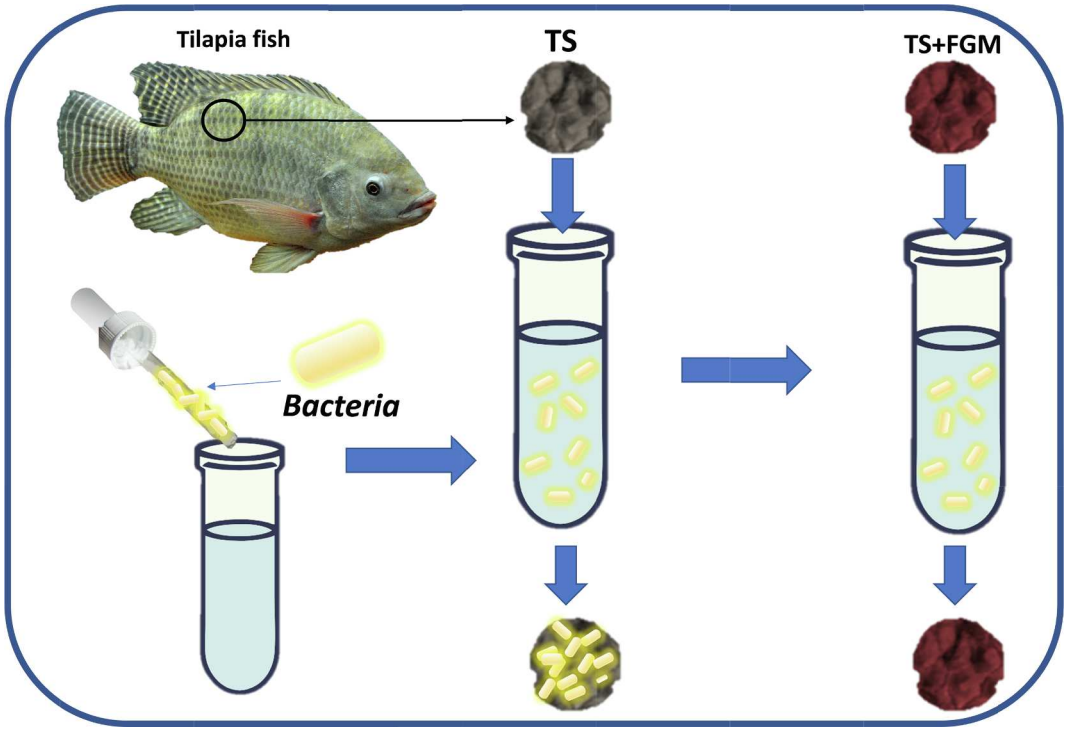

Fig. 1. General scheme describing the activity of the functional graphenic material (FGM) coating on active tilapia skin (TS). FGM-modified tilapia skin (TS + FGM, depicted in red) prevents bacterial adhesion. (For interpretation of the references to colour in this figure legend, the reader is referred to the web version of this article.)

2. Materials and methods

2.1. Materials

Tryptic soy broth (TSB) – (Fluka), Mueller-Hinton Agar (Himedia), phosphate buffered saline (PBS) and plate counter agar (PCA) (Aldrich), crystal violet (Proquimios), ethyl alcohol and acetone (Vetec) were used as received. Milli-Q water was used in all of the assays. Nile tilapia (*Oreochromis niloticus*) fish skins were donated by Omega Pescados do Vale (Brazil). Graphite flakes (-325 mesh, 99.8% metal basis), triethyl orthoacetate, trifluoroacetic acid (TFA), HBr (48% in H_2O), N, N-diisopropylethylamine (DIEA), and NaOH were obtained from Alfa Aesar and used as received. Concentrated H_2SO_4, 30% H_2O_2, and glacial acetic acid were obtained from Fisher Scientific and used as received. Hexylamine, $SOCl_2$, $KMnO_4$, *p*-toluene sulfonic acid, and all organic solvents (dioxane, acetone, dichloromethane (DCM), diethyl ether, dimethylformamide (DMF), tetrahydrofuran (THF), and ethanol) were obtained from Sigma-Aldrich. Dioxane, DMF, and THF were dried by passing through a column of activated alumina, then degassed with dry N_2 before use. SnakeSkin^{TM} dialysis tubing was obtained from Thermo Scientific and triphosgene was obtained from TCI America. N_6-carbobenzyloxy-L-lysine (Chem-Impex) was used to synthesize Lysine(Z)-NCA according to standard literature procedure [33].

2.2. Tilapia skin sterilization

Nile tilapia skins were transported in iceboxes to the Laboratory of Impedance Spectroscopy of Organic Materials (Univasf, Juazeiro, Brazil) and treated as follows: the excess of meat was carefully removed from the skin with a stiletto. After that, disks with 2 cm of diameter were cut from the tilapia skin and washed several times with milli-Q water. Tilapia skin was sterilized by immersion in a phosphate-buffered saline (PBS) solution (1x), followed by immersion in a 70% alcohol in water solution. Then, the material was left under ultraviolet light for 15 min to ensure complete sterilization in a procedure adapted from Refs. [2,34]. After sterilization, the tilapia skin was stored at a low temperature (2℃).

2.3. Synthesis of functional graphenic materials (FGMs)

FGMs (GO, CG, and PLL-G) were synthesized and characterized according to a published protocol [32]. Supplemental FGM characterization, including FTIR (Fig. S4), XRD (Fig. S5), and TEM (Fig. S6), is given in the supporting information (Figures S1-S5; Tables S1 and S2).

2.3.1. Synthesis of graphene oxide (GO)

GO was synthesized using a modified Hummer's method [35]. Briefly, graphite (7 g) was dispersed in concentrated H_2SO_4 (175 mL) in a 1 L flask. While stirring over ice, $KMnO_4$ (14 g) was slowly added to the reaction mixture over 30 min. The ice bath was removed, and the reaction was stirred for 2 h while warming to room temperature. Then, the reaction was gently heated to 35 °C and stirred for an additional 2 h. The heat was removed, and the reaction was quenched by quickly adding 980 mL of ice-cold deionized (DI) water, 30% H_2O_2 (15 mL), and then 315 mL of DI water. The reaction was then stirred overnight. To purify the GO, the reaction solution was vacuum filtered through a Büchner funnel fitted with coarse filter paper (VWR grade 415). The resulting GO monolith was carefully removed from the funnel without scraping the filter paper, loaded into dialysis tubing (3500 molecular weight cutoff), and dialyzed against DI water for 4 days. The dialysis water was changed twice per day. Then, the dialyzed GO was frozen to –80 °C and lyophilized for 3–5 days until dry.

2.3.2. Synthesis of Claisen graphene (CG)

CG was synthesized as previously described in Ref. [36]. Briefly, GO (5.8 g) and triethyl orthoacetate (1177 mL) were added to a flame dried, three-neck round bottom flask fitted with a condenser and bath sonicated (240 W, 42 kHz ultrasonic cleaner, Kendal) for 10 min. Then, *p*-toluene sulfonic acid (99 mg) was added, and the reaction was refluxed (143 °C) with stirring under a bed of N_2. After 36 h at reflux, the reaction was removed from heat, and 236 mL of 1 M NaOH (in DI water) was added with rapid stirring. After stirring at room temperature for an additional 11 h, the reaction solution was vacuum filtered. The CG monolith was transferred to a beaker containing 100 mL of DI water, sonicated for 10 s, then vacuum filtered again. The washing procedure was repeated twice with DI water, twice with ethanol, and twice with acetone. The purified CG was then dried under vacuum overnight and stored in a desiccator.

2.3.3. Synthesis of (poly-L-lysine)$_7$-G (PLL-G)

CG (1.2 g) and dry dioxane (1226 mL) were added to an oven-dried round bottom flask and sonicated for 10 min (240 W, 42 kHz, ultrasonic cleaner, Kendal) under a bed of N_2. Next, dry DMF (1.2 mL) and $SOCl_2$ (7.0 mL) were added dropwise while stirring vigorously under N_2. After stirring for 15 h at room temperature, the reaction solution was quickly vacuum filtered and rinsed with dry DCM (under ambient conditions). The resulting filter cake of ECG (electrophilic Claisen graphene) was immediately used for peptide endcapping (described in the next paragraph).

Poly(L-lysine-Z) (PLL(Z)) was synthesized concurrently. Lysine(Z)-NCA (1.29 g, 4.2 mmol) was added to an oven-dried round bottom flask, vacuum backfilled thrice with N_2, then dissolved in dry DMF (9.25 mL). Next, hexylamine (0.6 mmol) was added from a stock solution in dry DMF. After stirring for 10 min under N_2, the polymerization was placed under a light vacuum (approximately 300 mbar). Consumption of the NCA monomer was monitored by Fourier transform infrared spectroscopy, as indicated by the disappearance in anhydride peaks at 1855 and 1811 cm^{-1}. Following complete consumption of the monomer (approximately 2 h), dry DCM (9.25 mL), DIEA (2 mL), and the entire ECG filter cake (approx. 1.2 g) were added to the polymerization solution resulting in the production of white smoke. The reaction solution was sonicated for 10 min, then stirred at room temperature for two days under a bed of N_2. The reaction was then vacuum filtered, and the filtrate (containing unconjugated peptide) was reserved for GPC and ^1H NMR analysis (Figure S1). The product, a black solid, was rinsed several times with DMF, DI water, acetone, and DCM to eliminate unconjugated peptides and reaction byproducts. The resulting product, PLL(Z)-G, was dried under vacuum overnight.

To remove the Z protecting group from the conjugate material, PLL (Z)-G (1 g) was dispersed in glacial acetic acid (12 mL) via sonication (10 min). TFA (3 mL) and 48% aqueous HBr (2.8 mL) were added to the dispersion, and the reaction was stirred at room temperature for 48 h. The resulting reaction solution was centrifuged at 2160 × g for 10 min and the supernatant discarded. The pellet was washed by resuspension in the solvent, centrifugation at 2160 × g for 10 min, and decanting to discard the supernatant. Wash steps were performed four times with DI water, twice with acetone, and twice with diethyl ether. All supernatants from wash steps were discarded. The resulting deprotected PLL-G pellet was dried under vacuum overnight and stored in a desiccator. The scheme of PLL-G preparation is summarized in Fig. 2. Complete details about the FGM characterization are shown in Supporting Information (Figs. S1 to S3 and Tables S1 and S2).

2.4. Incorporation of FGM into tilapia skin

Sterile disks of tilapia fish were dried at ambient temperature and impregnated with either GO, CG, or PLL-G. FGM-based solutions were prepared by dispersing 60 mg of FGM in 10 mL of alcohol. Then, the FGM-based solution + skin disks were sonicated for 150 min. After the sonication process, the skins were removed from the FGM-based solutions, washed with ultrapure water, and dried at room temperature. Photos of the FGM-modified tilapia skins are shown in Fig. S7. SEM images of unmodified tilapia skin and FGM-modified tilapia skins are

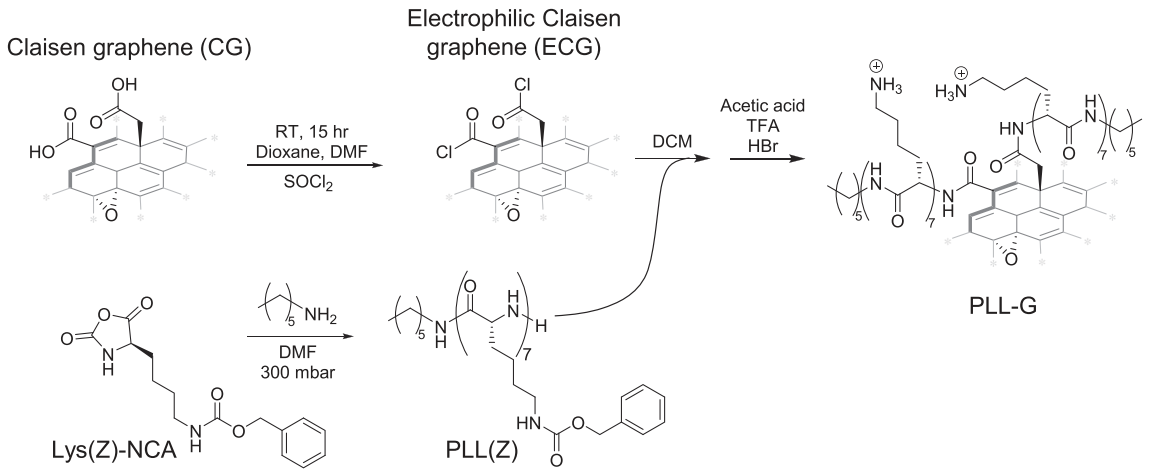

Fig. 2. Schematic representation of PLL-G synthesis. Bolded bonds represent graphenic sheet edges, and asterisks (*) indicate where the basal plane extends beyond the depicted structure.

shown in Fig. S8. The morphology of the tilapia skin surface is shown in Fig. S9a, and the surface of CG sheets is shown in Figs. S9b and S9c. AFM topographic images for unmodified tilapia skin (TS) and FGM-modified tilapia skins show a curved skin profile with variations in the maximum height from 590 to 1600 nm, which is a typical morphology of tilapia skin (Fig. S10). Notably, AFM topographic images indicate that incorporation of FGM into the tilapia skin surface increases the rugosity of the surface, compared to unmodified tilapia skin (Fig. S10).

2.5. Preparation of FGM pellets (control experiments)

FGM pellets were prepared and applied in a biological assay to serve as a comparison between the intrinsic response of the FGM additive and the antibiofilm and antibacterial activity of FGM-modified tilapia fish. Here, 600 mg of GO, CG, and PLL-G were pressed in a hydraulic press (10 kN). Photos of the FGM pellets are shown in Fig. S11. SEM images of the resulting structures are shown in Fig. S12.

2.6. Inhibition halo and kill time assays

The agar diffusion assays were performed for bacterial cultures of *Staphylococcus aureus* (ATCC 25923), *Klebsiella pneumoniae* (ATCC 13883) and *Escherichia coli* (ATCC 25922) that were dispersed in saline solution (0.5 of turbidity in McFarland scale). Aliquots of 10 μL of each solution were inoculated on Muller-Hinton agar (MHA) plates (experiments in triplicate). Then, FGM-modified tilapia skin disks were aseptically deposited on the MHA plate. After that, the plates were incubated at 37 °C for 24 h for the following registration of the inhibition zones. For kill time assays, reactors with 5 mL of TSB and 10^6 CFU/mL of each bacteria received FGM-modified tilapia skin disks. Aliquots of 100 μL from reactors were removed at a fixed interval of time from 0 h to 6 h and dispersed onto plate count agar (PCA). After incubation at 37 °C for 24 h, the counting of viable colonies was provided.

2.7. Biofilm formation assays on modified tilapia fish and pellets of FGMs

Staphylococcus aureus (ATCC 25923) and *Klebsiella pneumoniae* (ATCC 13883) were cultivated in PCA. Colonies were transferred to 20 mL of tryptic soy broth (TSB) to prepare a suspension in 0.5 McFarland standard scale (1.5×10^8 CFU/mL). After that, five test reactors each containing bacterial solutions were separated and received pure and FGM-modified tilapia skins (impregnated with either GO, CG, or PLL-G). The same procedure was established for pellets of FGMs that were introduced in three different reactors containing *S. aureus* and *K. pneumoniae* (the last reactor served as a control, containing the bacterial solution). For this, biofilm-forming strains of *S. aureus* and *K. pneumoniae* were inoculated for 24 h at 37 °C until to reach the required condition to form mature biofilms. The biofilm-forming quantification was provided by crystal violet retention assays, described in Section 2.7.1. This experiment was performed in triplicate. Data is presented as average of the three results, and error bars represent the standard deviation of the three results. To provide an alternative technique that confirms the obtained results by crystal violet staining, the direct counting of viable cells from biofilms was evaluated according to the procedure described in SI (Section S2.5).

2.7.1. Crystal violet retention assays

After the pre-established period for the biofilm maturation, the solution was removed and the reactors were washed with water to remove planktonic free-floating cells (weakly attached cells on walls of the reactor). The reactors and samples (disks of FGM-modified tilapia skin and FGM pellets) were washed three times with ultrapure water. After this step, the reactors and the samples (modified tilapia skin and pellets) were stained with 1% (w/v) crystal violet for 3 min, then carefully rinsed with water to remove unstained species. Finally, the stained biofilms were decolorized by the addition of an alcohol-acetone solution (80–20). Quantification of adhered biofilm on the reactor and sample surfaces was performed from direct measurement of the absorbance at the characteristic dye wavelength (570 nm – OD570) to determine the relative concentration of biofilm formation by Beer-Lambert law [31,37].

3. Results and discussion

Bacterial adhesion and repulsion can be influenced by charged surfaces, wherein the negatively charged bacterial cell wall participates in electrostatic interactions with the surface [38]. Electrostatic attraction between a positively charged polymer and negatively charged bacteria is the key physical principle behind the antibacterial activity of antibiotic-free agents (such as conducting polymers) [27-29,31]. These positively charged materials attract organisms towards the charged surface, then diffuse toxic compounds in the direction of the bacterial cells. The overall process (attachment of organisms, rupture of their cell wall structure, and diffusive process of reactive species) inhibits the viability of cellular mechanisms, as observed in silver-based antibacterial systems [30]. On this basis, a material with controllable surface charge could be implemented as a platform to direct bacterial adhesion (with positive surface charge) or to repel bacteria (with negative surface charge).

Functional graphenic materials (FGMs) are a promising class of

materials to fill this niche because their surface charge can be modulated by installing charged functional groups through covalent chemical modifications of the graphenic surface. In this study, FGMs with varying surface charge – graphene oxide (GO), Claisen graphene (CG), and poly-L-lysine-graphene (PLL-G) (structures and zeta potentials depicted in Fig. 3a) – were explored as coatings for tilapia skin (TS) wound dressing prototypes that rely on the electrostatic charge to prevent biofilm formation without the use of conventional antibiotics.

3.1. Functional graphenic material (FGM) charge is dictated by surface functional groups

The zeta potentials of the FGMs are a result of the identity and quantity of acidic or basic functional groups that are anchored on the graphenic sheet, which can be validated by deconvolution of high-resolution X-ray photoelectron spectroscopy (XPS). GO bears acidic carboxylic acids on the graphenic sheet edges, giving this FGM a net negative surface charge of −42.24 mV. CG is a derivative of GO that bears additional carboxylic acids on its basal plane, giving a larger magnitude of negative charge (-49.15 mV) compared to GO. This difference in the magnitude of negative charge can be explained by comparing the absolute atomic percent of carbons participating in a carboxylic acid (anionic), which can be extrapolated from the high-resolution C1s XPS spectra (Fig. 3b). Here, CG has 3.50% carboxylic acid carbons, compared to GO which has 2.02% carboxylic acid carbons, thus supporting the observed difference in zeta potential between these FGMs. On the other hand, PLL-G is made by conjugating a poly-L-lysine to CG through the carboxylic acids on CG, resulting in a graphenic surface bearing positively charged amines (+24.91 mV). The presence of amine (NH_2) and ammonium (NH_3) functional groups (cationic) in the high-resolution N1s XPS spectra of PLL-G demonstrates the source of its positive zeta potential (Fig. 3c).

3.2. Biocompatibility of FGMs and FGM-modified tilapia skins with mammalian and planktonic bacterial cells

The biocompatibility of the FGMs used in this work (GO, CG, and PLL-G) were previously evaluated with mammalian cell lines that are critical for wound healing (murine NIH-3 T3 fibroblasts), tissue regeneration (hMSCs), and immune function (murine RAW 264.7 macrophages). This previously reported data demonstrates that the FGMs exhibit dose-dependent cellular vitality with acceptable biocompatibility until the limit of high dose (>10 μg mL^{-1}) [39]. At higher FGM doses (>10 μg mL^{-1}), cellular toxicity can be attributed to the progressive smothering of graphenic materials on cells which may perturb the cell membrane and block access to nutrients and dissolved gases [40]. Based on this information, the FGMs reported herein can be utilized in biomedical materials with little to no deleterious effects on mammalian cells.

The biocompatibility of the FGMs (both as dispersions and as three-dimensional constructs) were also previously evaluated with gram-negative *E. coli* and gram-positive *B. subtilis*. Here, the FGMs (GO, CG, and PLL-G) were found to be biocompatible with both bacterial strains at dispersion concentrations up to 1000 μg mL^{-1}, albeit gram-positive bacteria were found to be more susceptible to FGM exposure [32]. Likewise, planktonic bacteria exposed to three-dimensional FGM pellets were found to have equal proliferation and viability compared to an untreated control [32].

In this work, the biocompatibility of FGM-modified tilapia skins was evaluated using inhibition halo and colony counting assays with gram-negative (*E. coli* and *K. pneumoniae*) and gram-positive (*S. aureus*) bacterial strains. In the inhibition halo experiments, negligible diffusion of active antibacterial agent is observed for CG, GO, and PLL-G-modified tilapia skins, as seen by the lack of an inhibition halo around these specimens in Fig. 4a (against *S. aureus*), Fig. 4b (against *E. coli*), and Fig. 4c (against *K. pneumoniae*). Notably, despite the well-established antibacterial activity of poly-L-lysine (PLL) in the free state, covalent conjugation of PLL to CG giving PLL-G, inhibits the diffusion of antibacterial species and suppresses the antibiotic activity of the conjugated PLL [32]. As such, no inhibition halo is observed around the PLL-G-modified tilapia skin (Fig. 4a-c). The overall antibacterial activity of the FGM-modified tilapia skins (impregnated with GO, CG, or PLL-G) was also monitored by counting viable cells after a fixed interval of treatment time. For all of the treatment times (from 0 h to 6 h) and all of

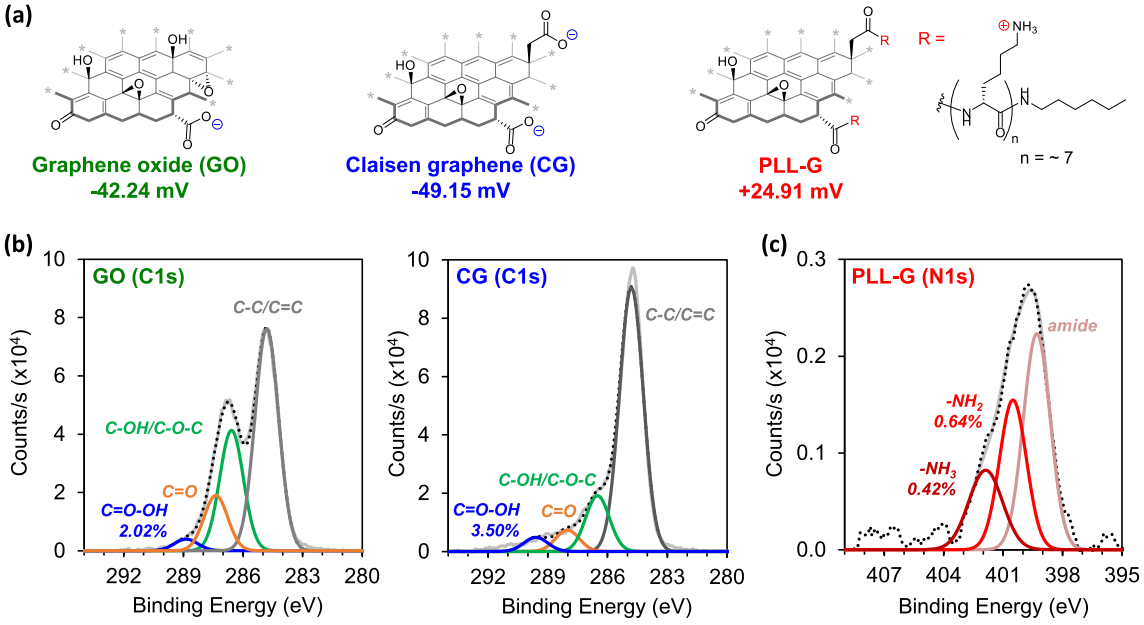

Fig. 3. (a) Functional graphenic materials (FGMs) (GO, CG, and PLL-G) have different zeta potentials based on their acidic and basic functional groups. (b) High-resolution C1s XPS was deconvoluted to determine the absolute atomic percent of carboxylic acids (C═O—OH) present in the negatively charged FGMs (GO and CG). CG has more carboxylic acids than GO (3.50% in CG versus 2.02% in GO), supporting its higher magnitude of negative zeta potential. (c) High-resolution N1s XPS of PLL-G was deconvoluted to demonstrate the absolute atomic percent of amine (—NH_2) and ammonium (—NH_3) functional groups (0.42% and 0.64%, respectively), which contribute to the positive zeta potential of PLL-G.

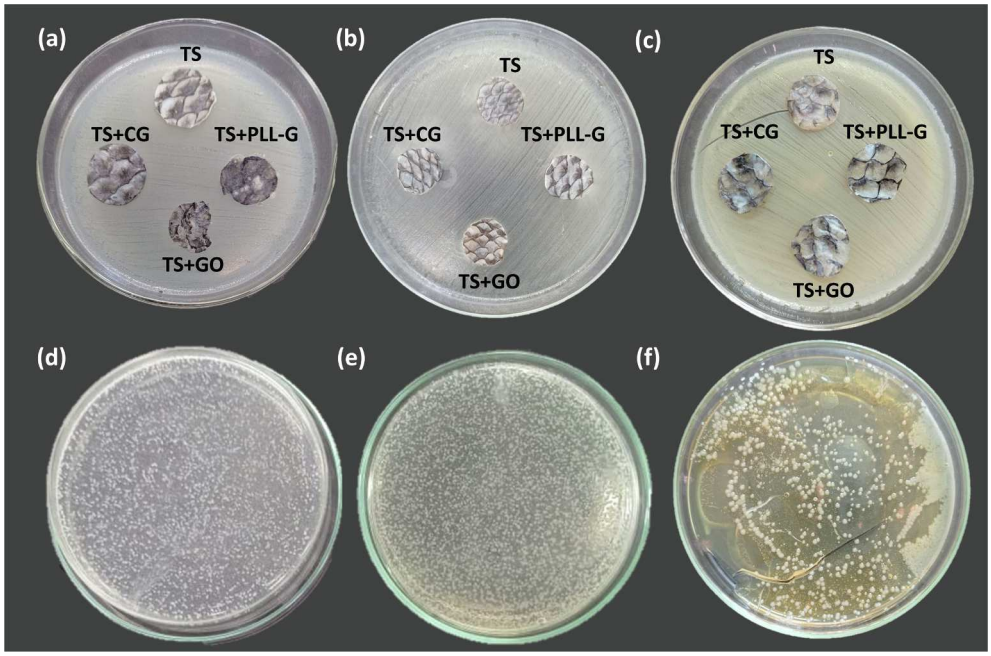

Fig. 4. Inhibition halo for TS an FGM-modified TS against *S. aureus* (a), *E. coli* (b), *K. pneumoniae* (c) and example of viable cells amount of *S. aureus* (d), *E. coli* (e) and *K. pneumoniae* (f) after treatment with TS and FGM-modified TS.

the compositions (TS + FGM), there was a negligible variation in the viable cell counts, which indicates the free growth of bacteria in the presence of pure and FGM-modified tilapia fish skins (Fig. 4d-f). Taken together, these results reinforce the absence of antibacterial activity of the FGM-modified tilapia skins towards planktonic bacteria.

The antibacterial activity of GO and its derivatives is widely debated: some reports have demonstrated that GO is nontoxic to bacteria [41,42], while others assert that GO has inherent antibacterial properties [43]. Our data indicates that the FGMs exhibit negligible toxicity towards planktonic gram-negative and gram-positive bacteria. We propose that the antibacterial activity of FGMs depends largely on the degree of contact between the bacteria and the FGM, which can be explained by the mechanism of antibacterial activity. One of the primary mechanisms of graphenic materials' antibacterial activity is the "nanoblade" effect, wherein the sharp edges of the graphenic material can puncture the cell walls of bacteria that are in direct contact [43]. SEM of the FGM powders and pellets demonstrate the presence of sharp edges on the flakes (Fig. S9 and S12), which could result in antibacterial activity towards bacteria in close contact with the FGM flakes (i.e.: biofilm bacteria). However, the inhibition halo and colony counting experiments analyzed in this section (Section 3.2) evaluate the viability of planktonic bacteria that had less direct contact with the sharp edges of the FGM flakes, compared to bacteria adsorbed directly to the FGM surface. Thus, we observed that the FGMs did not exhibit antibacterial activity towards

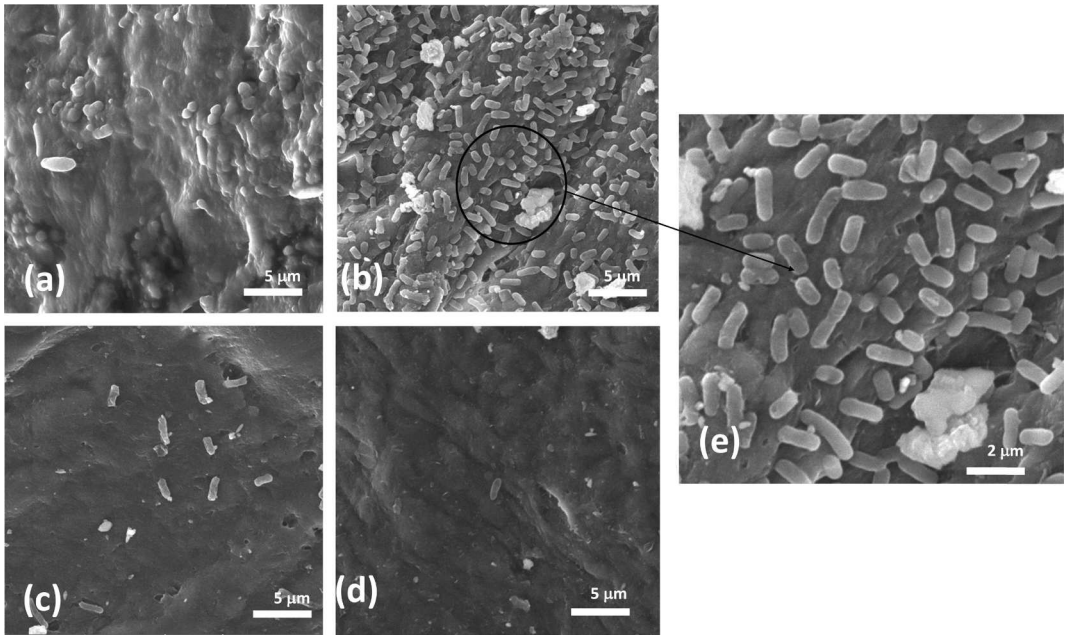

Fig. 5. SEM images of pure tilapia fish (a), and modified tilapia fish with PLL-G (b), GO (c) and CG (d) after contact with *E. coli* in a nutritive solution for 24 h at 37 ℃. Higher magnification for a zone of PLL-G-based sample is shown in panel (e).

these planktonic bacteria.

3.3. Qualitative analysis of bacterial adhesion to FGM-modified tilapia skins via SEM

The deposition and growth of bacteria on pure and modified tilapia skin was monitored using scanning electron microscopy (SEM) for different bacterial strains (*S. aureus*, *E. coli* and *K. pneumoniae*). A high density of viable *E. coli* cells was visible on pure tilapia skin, confirming the favorable conditions for bacterial growth (Fig. 5a). Impregnation of tilapia skin with the positively charged FGM (PLL-G) facilitates the electrostatic attraction with negatively charged bacterial species allowing dense deposition of viable bacterial cells (Fig. 5b and 5e) that confers additional risks for contamination of patient. On the other hand, as expected, tilapia skin impregnated with negatively charged FGMs – GO and CG, shown in Fig. 5c and 5d, respectively – introduce a strong repulsive activity against the adhesion of planktonic forms of *E. coli*, representing an advantageous property for wound dressing systems that could be applied in prolonged treatment against burns. These aspects were also observed for a gram-negative biofilm-forming model system (*K. pneumoniae*): SEM images in Fig. S13 confirm the previous observation that positively charged PLL-G-based tilapia skins attract bacterial species due to the electrostatic interaction, making a dense distribution of adhered cells compared to bacterio-repulsive, negatively charged tilapia skins (impregnated with GO or CG).

Similarly, following *S. aureus* exposure, the SEM images for pure tilapia skin revealed the presence of isolated sites in which aggregates of bacterial cells proliferate (Fig. 6a). Bacterial adhesion to the tilapia skin substrate is favored following impregnation with positively charged PLL-G, which attracts a dense distribution of *S. aureus* aggregates (Fig. 6b and 6e). The response of *S. aureus* adhesion to negatively charged modified tilapia skins (GO in Fig. 6c and CG in Fig. 6d) confirms the behavior observed against *E. coli*: a strong reduction in the bacterio-adhesive behavior is observed for GO and CG-modified tilapia skins with the best performance for CG-TS, in which scarce viable cells are observed.

These results offer a promising, qualitative analysis of the adhesion behavior of bacteria to the FGM-modified tilapia skin, which demonstrates that bacterial adhesion to the FGM-modified tilapia skins is dependent on the electrostatic charge of the FGM. To determine the degree of biofilm formation on these FGM-based surfaces, quantitative analysis of bacterial biofilm formation was performed and discussed in the next section. This study was separated into two parts, in which the intrinsic activity of pure FGMs (in pellet form) is evaluated as a control experiment for comparison with results observed for FGM-modified tilapia fish structures.

3.4. Antibiofilm activity of FGM pellets (control experiments)

For comparison of the antibiofilm properties of FGMs, experiments were conducted in triplicate to quantify the degree of *S. aureus* biofilm formation on tilapia skin (control) compared to pure FGM pellets. The degree of biofilm formation was evaluated by staining adhered (biofilm) bacteria with crystal violet and measuring the absorbance of the dye marker, where a higher absorbance of crystal violet indicates a higher degree of biofilm formation. The relative reduction in the biofilm formation (RBF) for each test sample was obtained by comparison with the control sample (unmodified tilapia skin) according to the following calculation:

$$\%ofRBF = 100^{*}\left(\frac{A_{570} - AC_{570}}{AC_{570}}\right) \quad (1)$$

where A_{570} = the absorbance at 570 nm of the test sample,

AC_{570} = the absorbance at 570 nm of the control sample (unmodified tilapia skin)

After 24 h of exposure to *S. aureus* in a reactor, all of the FGM pellets – regardless of their charge – strongly reduce the biofilm formation of *S. aureus* compared to tilapia skin (Fig. 7a), indicating that the FGM pellets possess antibiofilm properties. The charge of FGM pellets had a negligible effect on the amount of biofilm formed on the reactor surface, indicating that the antibiofilm properties of the FGM pellets are localized to the pellet surface (Fig. S14a and S14b). The mechanism of antibiofilm activity is expected to be influenced by two properties: 1) the morphology of the FGM pellet surface and 2) the surface charge of the

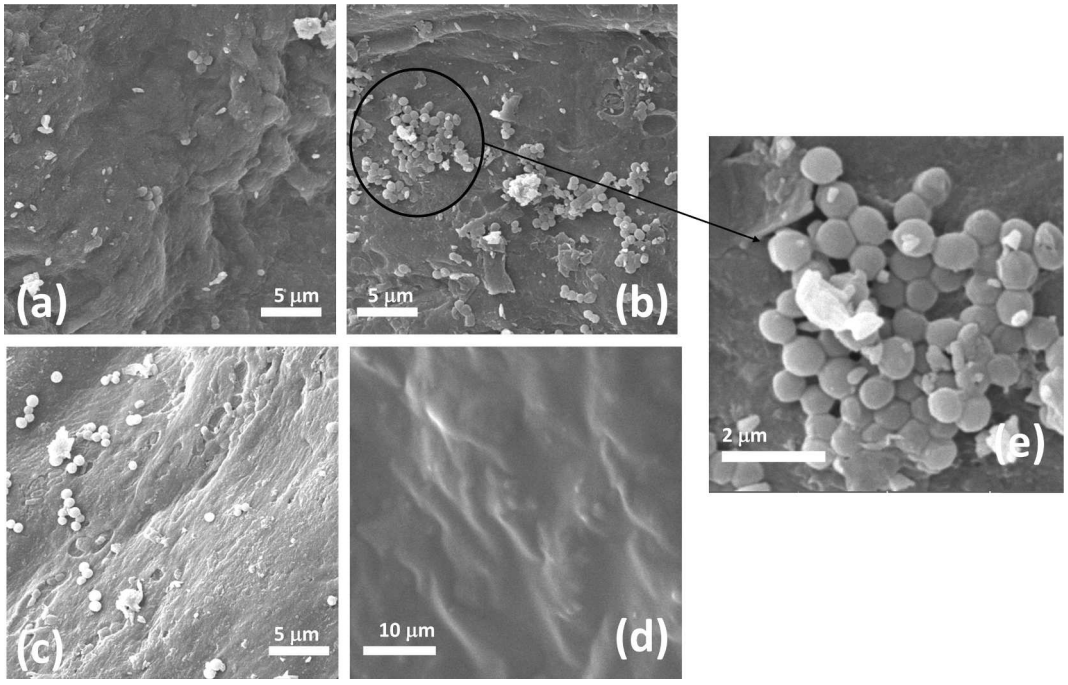

Fig. 6. SEM images of pure tilapia fish (a), and modified tilapia fish with PLL-G (b), GO (c) and CG (d) after contact with *S. aureus* in a nutritive solution for 24 h at 37 ℃. Higher magnification for a zone of PLL-G-based sample is shown in panel (e).

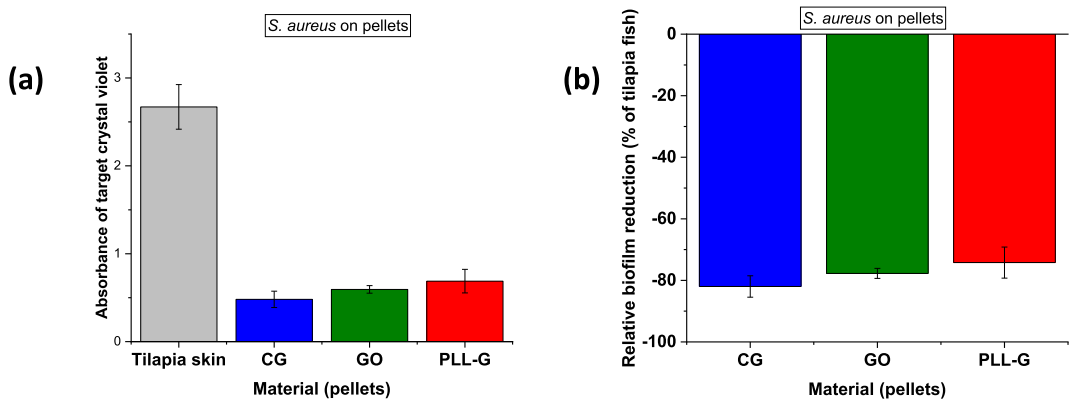

Fig. 7. The absorbance of crystal violet stain (λ_{max} = 570 nm) can be used to quantify and compare the absolute (a) and relative (b) amount of *S. aureus* biofilm on the surface of a tilapia skin substrate versus bulk FGM pellets (CG, GO, and PLL-G). (For interpretation of the references to colour in this figure legend, the reader is referred to the web version of this article.)

FGM.

FGM morphology was evaluated using SEM of the bulk FGM pellets, which demonstrates the presence of corners and sharp edges protruding from the pellet surface (Fig. S12). This jagged morphology may contribute to antibacterial activity through membrane puncturing, a mechanism of GO antibacterial activity that has been proposed in the literature [44]. Given this, antibiofilm activity of the FGM pellets may be due, in part, to bacterial toxicity from direct physical contact with the biofilm bacterial and subsequent "nanoblade" effect when the FGM flakes puncture the cell wall. It is important to note that this antibacterial activity was not observed towards planktonic bacteria that had less direct contact with the FGM flakes, compared to the biofilm bacteria (Fig. 4).

The charge of the FGM pellet is an additional driving force that defines the order of bacterial adhesion to the surface. We found that relative reduction of biofilm follows the order: CG (81.98%) > GO (77.74%) > PLL-G (74.22%) (Fig. 7b). This trend in biofilm repulsion performance is justified by the net charge of each compound (zeta-potential values of −49.15 mV for CG, −42.24 mV for GO, and + 24.91 mV for PLL-G) (Fig. 3). Notably, the negatively charged FGM pellets (GO and CG) demonstrate the best antibiofilm performance with dual activity from 1) repulsive forces between the negatively charged FGM surface and bacterial cell wall, and 2) nanoblade effect as the jagged pellet surface punctures bacterial cell walls on contact. On the other hand, positively charged PLL-G pellets have weaker antibiofilm performance, compared to negatively charged GO and CG pellets. Previous research has demonstrated that while positively charged surfaces act as an attractive support for bacterial adsorption [45], they can also limit bacterial proliferation and viability depending on the magnitude of charge [46,47]. Strong bacterial adhesion can prevent elongation – an essential step in cell division [48,49]. With this in mind, we propose that the antibiofilm activity of the PLL-G pellets can be attributed to 1) attractive forces with negatively charged bacteria that adsorb bacteria and suppress their proliferation, and 2) nanoblade effect with biofilm bacteria that are in direct contact with the pellet surface.

3.5. Antibiofilm activity of FGM-modified tilapia skins

The impregnation of FGMs in tilapia fish skin introduces the mutual advantages of intrinsic biological activity of both the tilapia skin and FGM components, while also imparting antibiofilm properties from the FGM component. As such, we quantified the deposition of *S. aureus* and *K. pneumoniae* biofilms on pure tilapia skins (control) compared to tilapia skins impregnated with the FGMs following 24 h exposure to bacteria (all of the experiments were performed in triplicate). Absolute and relative biofilm formation was determined quantitatively using the crystal violet assay, as described above in Section 3.4. As a confirmation study, we also quantified viable cell counts in the biofilms by extracting the biofilm bacteria from the scaffold surface via sonication and performing colony counting assays (Supporting Information, Section S2.5).

When evaluated with gram-positive *S. aureus*, negatively charged bacterio-repulsive FGMs (CG- and GO- modified TS) contribute to a strong reduction in the biofilm formation on tilapia skin (88.8% for CG, 84.9% for GO) (Fig. 8). Meanwhile, positively charged, bacterio-adhesive PLL-G reduces biofilm formation on tilapia skin to a lesser degree (76.1% for PLL-G). These results (obtained by crystal violet staining) are supported by the colony counting assay, which demonstrates a reduction of viable cells in the biofilms on the FGM-modified tilapia skins, compared to the unmodified tilapia skins (Fig. S15a and S15b).

Corresponding experiments were conducted to quantify the degree of gram-negative *K. pneumoniae* biofilm formation on FGM-modified tilapia skin samples. These experiments confirm the same behavior observed against gram-positive *S. aureus*: FGM-modified tilapia skins exhibit reduced biofilm deposition compared to tilapia skins alone, and the magnitude of biofilm reduction (most-to-least biofilm reduction – CG > GO > PLL-G) corresponds to the order in FGM zeta-potential (more negative to more positive species) (Fig. 9). Again, the colony counting assay supports the assertion that FGM-modification reduces the bacteria biofilm on the tilapia skins, particularly in the case of bacterio-repulsive, negatively charged CG- and GO-modified tilapia skins (Fig. S15c and S15d).

The FGM-modified tilapia skins exhibit lower activity against gram-negative *K. pneumoniae* (in the range of 40.6–49.7% biofilm reduction), compared to their activity against gram-positive *S. aureus* (in the range of 88.8% – 76.1% biofilm reduction) – a trend that has been previously observed in the literature [50,51]. This difference in antibiofilm performance against gram-negative and gram-positive species can be attributed to differences in the structure – specifically, the outermost layer – of the bacterial cell walls (Fig. 10). For gram-negative bacteria, the outermost layer of the cell wall is an outer membrane, which provides an added layer of protection against interactions with sharp graphenic flakes [44]. On the other hand, gram-positive species lack a protective outer membrane and instead have a thick peptidoglycan layer with teichoic acid polymers anchored in the plasma membrane and extending beyond the cell wall [52]. It has been proposed that the peptidoglycan and lipoteichoic acid functionalities on the gram-positive bacteria surface facilitate stronger interactions – and thus greater contact – with graphenic materials, compared to the outer membrane of gram-negative species [50]. Overall, while the FGM-modified tilapia skin xenografts exhibit antibacterial properties against both gram-positive and gram-negative bacteria, the lack of a protected outer membrane and enhanced contact with sharp FGM flakes may contribute to the greater susceptibility of gram-positive bacteria, compared to

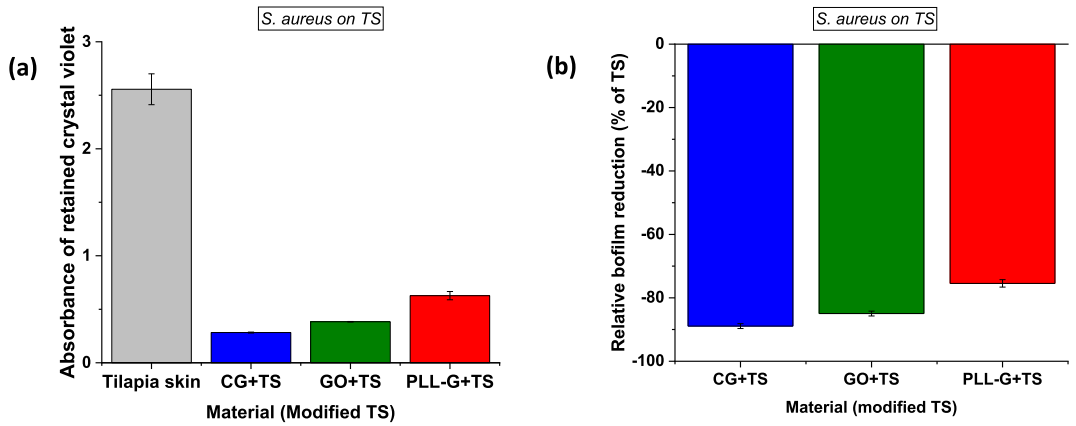

Fig. 8. The absorbance of crystal violet stain (λ_{max} = 570 nm) can be used to quantify and compare the absolute (a) and relative (b) amount of *S. aureus* biofilm on the surface of a tilapia skin substrate versus FGM-modified tilapia skins (CG + TS, GO + TS, and PLL-G + TS). (For interpretation of the references to colour in this figure legend, the reader is referred to the web version of this article.)

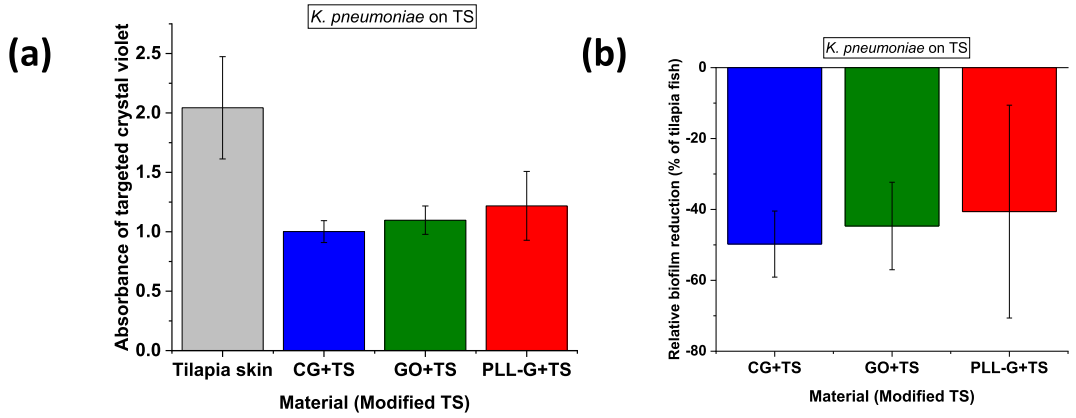

Fig. 9. The absorbance of crystal violet stain (λ_{max} = 570 nm) can be used to quantify and compare the absolute (a) and relative (b) amount of *K. pneumoniae* biofilm on the surface of a tilapia skin substrate versus FGM-modified tilapia skins (CG + TS, GO + TS, and PLL-G + TS). (For interpretation of the references to colour in this figure legend, the reader is referred to the web version of this article.)

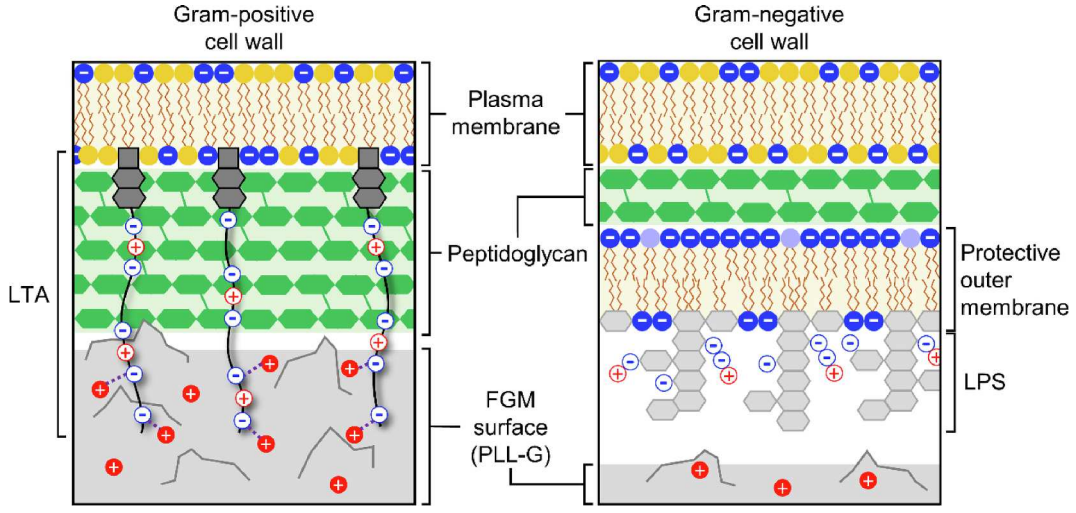

Fig. 10. (a) Graphical representation of a gram-positive and gram-negative cell wall is based on information from Malanovic and Lohner (LTA = lipoteichoic acid, LPS = lipopolysaccharide) [52]. Gram-positive bacteria lack a protective outer membrane. Enhanced interactions between charged LTA polymers in the gram-positive cell wall and the rough FGM surface leads to higher susceptibility towards the FGM, compared to gram-negative bacteria.

gram-negative bacteria.

Overall, this analysis demonstrated that, compared to unmodified tilapia skins, biofilm formation is reduced on all FGM-modified tilapia skins – regardless of charge – but that FGM surface does play a role in modulating the degree of biofilm reduction on the xenograft prototype. The results presented here reinforce the trends observed for the bulk FGM pellets, suggesting that both antibacterial activity of the FGMs (via nanoblade effect) and electrostatic interaction of the FGM with microorganisms contribute to the mechanism of antibiofilm activity of the FGM-modified tilapia skin xenografts. It is worth mentioning that the FGM-modified tilapia skins effectively reduce biofilm formation on the tilapia skin substrate using only a small amount of FGM powder, compared to bulk FGM pellets. As such, impregnating tilapia fish skin with FGMs represents a promising approach for production of low cost and large-scale bacterial repulsive dressings that could improve wound treatment outcomes by simultaneously accelerating wound healing and preventing bacterial biofilms.

4. Conclusions

In this work, tilapia fish skin xenografts were impregnated with functional graphenic materials (FGMs) possessing different surface charges as a strategy to impart antibiofilm properties to the xenograft surface. We found that all FGM-modified tilapia skins exhibited antibiofilm properties, compared to unmodified tilapia skin, regardless of their surface charge. This behavior is expected to be due to 2 properties: 1) FGMs possess sharp corners and edges that can kill biofilm bacteria via the nanoblade effect; and 2) electrostatic interactions with the FGM can either strongly adhere bacteria to suppress proliferation (PLL-G) or repel bacteria (GO and CG). Notably, the FGM surface charge impacts the degree of biofilm reduction. Compared to unmodified tilapia skin, tilapia skin that was impregnated with the most negatively charged FGM (CG + TS) exhibited the best antibiofilm performance (88.8% and 49.7% reduction of biofilm for *S. aureus* and *K. pneumoniae*, respectively), while tilapia skin impregnated with a positively charged FGM (PLL-G + TS) exhibited the weakest antibiofilm activity (76.1% and 40.6% reduction of biofilm for *S. aureus* and *K. pneumoniae*, respectively). These results suggest that electrostatic interactions between the charged FGM and the negatively charged bacterial membrane play a role in modulating the degree of biofilm reduction on the FGM-modified tilapia skins. The activity of CG-modified tilapia skin against biofilm bacteria represents an important feature in preventing infection in xenograft wound dressings, and demonstrates potential for prolonged use of FGM-modified tilapia skin to treat burns without the use of conventional antibiotics. The addition of an anti-biofilm FGM coating adds value to natural fish skin xenografts by providing an additional barrier against bacterial adhesion while also maintaining the low cost of implementation and the intrinsic healing properties of this natural support.

CRediT authorship contribution statement

Fernando Antonio Gomes da Silva: Methodology, Investigation, Writing – original draft. **Karoline E. Eckhart:** Methodology, Formal analysis, Investigation, Writing – original draft, Writing – review & editing. **Mateus Matiuzzi da Costa:** Methodology. **Stefanie A. Sydlik:** Conceptualization, Methodology, Formal analysis, Writing – review & editing, Funding acquisition. **Helinando Pequeno de Oliveira:** Conceptualization, Methodology, Formal analysis, Writing – original draft, Writing – review & editing, Funding acquisition.

Declaration of Competing Interest

The authors declare that they have no known competing financial interests or personal relationships that could have appeared to influence the work reported in this paper.

Acknowledgement

This work was partially supported by Brazilian funding agencies CAPES, FINEP, FACEPE (APQ-0444-1.05/20), and CNPq. We thank Joel Gillespie for providing training and use of the XPS in the Materials Characterization Laboratory at the University of Pittsburgh. The authors acknowledge Krzysztof Matyjaszewski (GPC, Zetasizer) and Roberto Gil (NMR, funded in part by NSF grant # CHE-9808188, CHE-1039870, and CHE1726525) for the use of their facilities. We thank Jason Orlando and Ted Pella for acquiring the TEM images. The authors acknowledge use of the Materials Characterization Facility at Carnegie Mellon University supported by grant MCF-677785.

Appendix A. Supplementary data

Supplementary data to this article can be found online at https://doi.org/10.1016/j.apsusc.2021.151768.

References

[1] E.M. Lima-Junior, M. Odorico, D.M. Filho, B.A. Costa, F.V. Fechine, M. Elisabete, A. De Moraes, F.R. Silva-junior, M. Flaviane, N. Soares, M. Becker, S. Rocha, C. Maria, P. Leontsinis, Innovative treatment using tilapia skin as a xenograft for partial thickness burns after a gunpowder explosion, J. Surg. Case Rep. 2019 (2019) 1–4, https://doi.org/10.1093/jscr/rjz181.

[2] E. Maciel, L. Júnior, M. Odorico, D.M. Filho, M. Becker, S. Rocha, F.V. Fechine, A. J. Forte, A. Paula, N. Nunes, F. Raimundo, S. Júnior, C.B. Martins, M.B. Mathor, Innovative Burn Treatment Using Tilapia Skin as a Xenograft : A Phase II Randomized Controlled, J. Burn Care Res. 41 (3) (2020) 585–592, https://doi.org/10.1093/jbcr/irz205.

[3] L.C. D'Avignon, B.K. Hogan, C.K. Murray, F.L. Loo, D.R. Hospenthal, L.C. Cancio, S. H. Kim, E.M. Renz, D. Barillo, J.B. Holcomb, C.E. Wade, S.E. Wolf, Contribution of bacterial and viral infections to attributable mortality in patients with severe burns: An autopsy series, Burns 36 (6) (2010) 773–779, https://doi.org/10.1016/j.burns.2009.11.007.

[4] M.P. Rowan, L.C. Cancio, E.A. Elster, D.M. Burmeister, L.F. Rose, S. Natesan, R. K. Chan, R.J. Christy, K.K. Chung, Burn wound healing and treatment: review and advancements, Crit. Care 191 (19) (2015) 1–12, https://doi.org/10.1186/S13054-015-0961-2.

[5] C.G. Mayhall, The epidemiology of burn wound infections: then and now, Clin. Infec. Dis. 37 (2003) 543–550, https://doi.org/10.1086/376993.

[6] A. Ibrahim, D. Hassan, N. Kelany, S. Kotb, M. Soliman, Validation of three different sterilization methods of tilapia skin dressing: impact on microbiological enumeration and collagen content, Front. Vet. Sci. 7 (2020) 5–8, https://doi.org/10.3389/fvets.2020.597751.

[7] E.M. Lima Junior, M.O. de Morais Filho, A.J. Forte, B.A. Costa, F.V. Fechine, A.P.N. N. Alves, M.E.A. de Moraes, M.B.S. Rocha, F.R. Silva Junior, M.F.A.N. Soares, A. N. Bezerra, C.B. Martins, M.B. Mathor, Pediatric burn treatment using tilapia skin as a xenograft for superficial partial-thickness wounds: a pilot study, J. Burn Care Res. 41 (2) (2020) 241–247, https://doi.org/10.1093/jbcr/irz149.

[8] O. Qianqian, K. Songzhi, H. Yongmei, J.u. Xianghong, L.i. Sidong, L.i. Puwang, L. Hui, International Journal of Biological Macromolecules Preparation of nano-hydroxyapatite / chitosan / tilapia skin peptides hydrogels and its burn wound treatment, Int. J. Biol. Macromol. 181 (2021) 369–377, https://doi.org/10.1016/j.ijbiomac.2021.03.085.

[9] C.O. Chantre, S.P. Hoerstrup, K.K. Parker, Engineering biomimetic and instructive materials for wound healing and regeneration, Curr. Opin. Biomed. Eng. 10 (2019) 97–106, https://doi.org/10.1016/J.COBME.2019.04.004.

[10] S. Hu, X. Cai, X. Qu, B. Yu, C. Yan, J. Yang, F. Li, Y. Zheng, X. Shi, International Journal of Biological Macromolecules Preparation of biocompatible wound dressings with long-term antimicrobial activity through covalent bonding of antibiotic agents to natural polymers, Int. J. Biol. Macromol. 123 (2019) 1320–1330, https://doi.org/10.1016/j.ijbiomac.2018.09.122.

[11] A.P.N.N. Alves, E.M. Lima Júnior, N.S. Piccolo, M.J.B. de Miranda, M.E.Q. Lima Verde, A.E.C. Ferreira Júnior, P.G. de Barros Silva, V.P. Feitosa, T.J.P.G. de Bandeira, M.B. Mathor, M.O. de Moraes, Study of tensiometric properties, microbiological and collagen content in nile tilapia skin submitted to different sterilization methods, Cell Tissue Bank. 19 (3) (2018) 373–382, https://doi.org/10.1007/s10561-017-9681-y.

[12] B.O. Costa, E.M.L. Júnior, F.V. Fechine, A.P.N.N. Alves, M.M.O. de Melo, W.L. C. Ribeiro, J.P. Siqueira, M.O.M. deFilho, Treatment of a traumatic equine wound using Nile tilapia (Oreochromis niloticus) skin as a xenograft, Acta Sci. Vet. 48 (2020) 1–6, https://doi.org/10.22456/1679-9216.99678.

[13] E.M. Lima Júnior, M.O. de Moraes Filho, B.A. Costa, A.P.N.N. Alves, M.E.A. de Moraes, A.M. do Nascimento Uchôa, C.B. Martins, T. de Jesus Pinheiro Gomes Bandeira, F.A.R. Rodrigues, C.R.K. Paier, F.C. Lima, F.R. Silva Júnior, Lyophilised tilapia skin as a xenograft for superficial partial thickness burns: a novel preparation and storage technique, J. Wound Care. 29 (10) (2020) 598–602, https://doi.org/10.12968/jowc.2020.29.10.598.

[14] G. Fiakos, Z. Kuang, E. Lo, Improved skin regeneration with acellular fish skin grafts, Eng. Regen. 1 (2020) 95–101, https://doi.org/10.1016/J.ENGREG.2020.09.002.
[15] S. Magnusson, B.T. Baldursson, H. Kjartansson, O. Rolfsson, G.F. Sigurjonsson, Regenerative and Antibacterial Properties of Acellular Fish Skin Grafts and Human Amnion/Chorion Membrane: Implications for Tissue Preservation in Combat Casualty Care, Mil. Med. 182 (S1) (2017) 383–388, https://doi.org/10.7205/MILMED-D-16-00142.
[16] A. Ibrahim, M. Soliman, S. Kotb, M.M. Ali, Evaluation of fish skin as a biological dressing for metacarpal wounds in donkeys, BMC Vet. Res. 16 (2020) (2020) 1–10, https://doi.org/10.1186/S12917-020-02693-W, 161.
[17] M.T.P.M. Dias, A.P.M. Bilhar, L.C. Rios, B.A. Costa, E.M. Lima Júnior, A.P.N. N. Alves, Z.V. Bruno, M.O. de Moraes Filho, L.R.P.S. Bezerra, Neovaginoplasty using Nile Tilapia Fish Skin as a new biological graft in patients with Mayer-Rokitansky-Küster-Hauser syndrome, J. Minim. Invasive Gynecol. 27 (4) (2019) 966–972, https://doi.org/10.1016/j.jmig.2019.09.779.
[18] R.S. Boneva, T.M. Folks, L.E. Chapman, Infectious Disease Issues in Xenotransplantation, Clin. Microbiol. Rev. 14 (1) (2001) 1–14, https://doi.org/10.1128/CMR.14.1.1-14.2001.
[19] G.C.C. Mendes, T.R.S. Brandão, C.L.M. Silva, Ethylene oxide sterilization of medical devices: A review, Am. J. Infect. Control 35 (9) (2007) 574–581, https://doi.org/10.1016/j.ajic.2006.10.014.
[20] B.P. Conrad, M. Rappe, M. Horodyski, K.W. Farmer, P.A. Indelicato, The effect of sterilization on mechanical properties of soft tissue allografts, Cell Tissue Bank 14 (2013) 359–366, https://doi.org/10.1007/s10561-012-9340-2.
[21] M.A. Metwally, S.S. Ali, I.A. Khatab, .M.K. El-Sayed, Antibacterial potential of some seaweeds species to combat biofilm-producing multi-drug resistant Staphylococcus aureus of Nile Tilapia, Egypt, J. Bot. 60 (1) (2020) 9–24, https://doi.org/10.21608/ejbo.2019.6829.1275.
[22] S. Kathju, L. Nistico, L.-A. Lasko, P. Stoodley, Bacterial biofilm on monofilament suture and porcine xenograft after inguinal herniorrhaphy, FEMS Immunol. Med. Microbiol. 59 (3) (2010) 405–409, https://doi.org/10.1111/j.1574-695X.2010.00691.x.
[23] L. Bi, Y. Hu, H. Fan, G. Meng, J. Liu, D. Li, R. Lv, Treatment of Contaminated Bone Defects With Clindamycin-Reconstituted Bone Xenograft-Composites, Wiley Online Libr. 82B (2) (2007) 418–427, https://doi.org/10.1002/(ISSN)1552-498110.1002/jbm.b.v82b:210.1002/jbm.b.30747.
[24] S. Busby, A. Robb, S. Lang, Y. Takeuchi, P. Vesely, L. Scobie, Antibiotic susceptibility and resistance of Staphylococcus aureus isolated from fresh porcine skin xenografts: risk to recipients with thermal injury, Burns 40 (2) (2014) 288–294, https://doi.org/10.1016/j.burns.2013.06.006.
[25] T.S.C. Mana, C. Donskey, N. Carty, L. Perry, D. Leaper, C.E. Edmiston, Preliminary analysis of the antimicrobial activity of a postoperative wound dressing containing chlorhexidine gluconate against methicillin-resistant Staphylococcus aureus in an in vivo porcine incisional wound model, Am. J. Infect. Control. 47 (9) (2019) 1048–1052, https://doi.org/10.1016/j.ajic.2019.05.012.
[26] R. Lima, F.S. Del Fiol, V.M. Balcão, Prospects for the Use of New Technologies to Combat Multidrug-Resistant Bacteria, Front. Pharmacol. (2019) 692, https://doi.org/10.3389/FPHAR.2019.00692.
[27] F.A.G. da Silva, J.J. Alcaraz-Espinoza, M.M. da Costa, H.P. de Oliveira, Low intensity electric field inactivation of Gram-positive and Gram-negative bacteria via metal-free polymeric composite, Mater. Sci. Eng. C. 99 (2019) 827–837, https://doi.org/10.1016/j.msec.2019.02.027.
[28] F.A.G. Da Silva, J.C. Queiroz, E.R. Macedo, A.W.C. Fernandes, N.B. Freire, M.M. Da Costa, H.P. De Oliveira, Antibacterial behavior of polypyrrole: The influence of morphology and additives incorporation, Mater. Sci. Eng. C. 62 (2016) 317–322, https://doi.org/10.1016/j.msec.2016.01.067.
[29] Ravi M.A.P. Lima, Jose Jarib Alcaraz-Espinoza, Fernando A.G. da Silva, Helinando P. de Oliveira, Multifunctional Wearable Electronic Textiles Using Cotton Fibers with Polypyrrole and Carbon Nanotubes, ACS Appl. Mater. Interfaces. 10 (16) (2018) 13783–13795, https://doi.org/10.1021/acsami.8b04695.
[30] M.L. Guimarães, F.A.G. da Silva, M.M. da Costa, H.P. de Oliveira, Green synthesis of silver nanoparticles using Ziziphus joazeiro leaf extract for production of antibacterial agents, Appl. Nanosci. 10 (4) (2020) 1073–1081, https://doi.org/10.1007/s13204-019-01181-4.
[31] M.R. dos Santos, F.A.G. da Silva, P.P. Ferrais, R.S. de Lima, M.M. da Costa, H.P. de Oliveira, Polyaniline-coated Calotropis procera L. hollow tubular fibers with remarkable antibacterial activity, SN, Appl. Sci. 2 (9) (2020), https://doi.org/10.1007/s42452-020-03345-2.
[32] K.E. Eckhart, A.M. Arnold, F.A. Starvaggi, S.A. Sydlik, Tunable, bacterio-instructive scaffolds made from functional graphenic materials, Biomater. Sci. 9 (7) (2021) 2467–2479, https://doi.org/10.1039/D0BM01471K.
[33] K.E. Eckhart, F.A. Starvaggi, S.A. Sydlik, One-Shot Synthesis of Peptide Amphiphiles with Applications in Directed Graphenic Assembly, Biomacromolecules. 21 (9) (2020) 3878–3886, https://doi.org/10.1021/acs.biomac.0c0096210.1021/acs.biomac.0c00962.s001.
[34] F. Howaili, M. Mashreghi, N.M. Shahri, A. Kompany, R. Jalal, Development and evaluation of a novel beneficent antimicrobial bioscaffold based on animal waste-fish swim bladder (FSB) doped with silver nanoparticles, Environ. Res. 188 (2020) 109823, https://doi.org/10.1016/j.envres.2020.109823.
[35] W.S.H. Jr., R.E. Offeman, Preparation of Graphitic Oxide, J. Am. Chem. Soc. 80 (2002) 1339. https://doi.org/10.1021/JA01539A017.
[36] S.A. Sydlik, T.M. Swager, Functional Graphenic Materials Via a Johnson−Claisen Rearrangement, Adv. Funct. Mater. 23 (15) (2013) 1873–1882, https://doi.org/10.1002/adfm.v23.1510.1002/adfm.201201954.
[37] T. Gobor, G. Corol, L.E.N. Ferreira, A.U.M. Rymovicz, R.T. Rosa, P.M.S. Campelo, E.A.R. Rosa, Proposal of protocols using D-glutamine to optimize the 2,3-bis(2-methoxy-4-nitro-5-sulfophenly)-5-[(phenylamino) carbonyl]-2H-tetrazolium hydroxide (XTT) assay for indirect estimation of microbial loads in biofilms of medical importance, J. Microbiol. Methods. 84 (2) (2011) 299–306, https://doi.org/10.1016/j.mimet.2010.12.018.
[38] S. Zheng, M. Bawazir, A. Dhall, H.-E. Kim, L. He, J. Heo, G. Hwang, Implication of Surface Properties, Bacterial Motility, and Hydrodynamic Conditions on Bacterial Surface Sensing and Their Initial Adhesion, Front. Bioeng. Biotechnol. (2021) 82, https://doi.org/10.3389/FBIOE.2021.643722.
[39] K.E. Eckhart, B.D. Holt, M.G. Laurencin, S.A. Sydlik, Covalent conjugation of bioactive peptides to graphene oxide for biomedical applications, Biomater. Sci. 7 (9) (2019) 3876–3885, https://doi.org/10.1039/C9BM00867E.
[40] Brian D. Holt, Anne M. Arnold, Stefanie A. Sydlik, The Blanket Effect: How Turning the World Upside Down Reveals the Nature of Graphene Oxide Cytocompatibility, Adv. Healthc. Mater. 10 (7) (2021) 2001761, https://doi.org/10.1002/adhm.v10.710.1002/adhm.202001761.
[41] O.N. Ruiz, K.A.S. Fernando, B. Wang, N.A. Brown, P.G. Luo, N.D. McNamara, M. Vangsness, Y.-P. Sun, C.E. Bunker, Graphene Oxide: A Nonspecific Enhancer of Cellular Growth, ACS Nano. 5 (10) (2011) 8100–8107, https://doi.org/10.1021/nn202699t.
[42] I. Barbolina, C.R. Woods, N. Lozano, K. Kostarelos, K.S. Novoselov, I.S. Roberts, Purity of graphene oxide determines its antibacterial activity, 2D Mater 3 (2) (2016) 025025, https://doi.org/10.1088/2053-1583/3/2/025025.
[43] P. Kumar, P. Huo, R. Zhang, B. Liu, Antibacterial properties of graphene-based nanomaterials, Nanomater 9 (2019) 737, https://doi.org/10.3390/NANO9050737.
[44] O. Akhavan, E. Ghaderi, Toxicity of Graphene and Graphene Oxide Nanowalls Against Bacteria, ACS Nano 4 (2010) 5731–5736, https://doi.org/10.1021/NN101390X.
[45] G. Harkes, J. Feijen, J. Dankert, Adhesion of Escherichia coli on to a series of poly (methacrylates) differing in charge and hydrophobicity, Biomaterials 12 (9) (1991) 853–860, https://doi.org/10.1016/0142-9612(91)90074-K.
[46] S. Some, S.-M. Ho, P. Dua, E. Hwang, Y.H. Shin, H. Yoo, J.-S. Kang, D. Lee, H. Lee, Dual Functions of Highly Potent Graphene Derivative–Poly-l-Lysine Composites To Inhibit Bacteria and Support Human Cells, ACS Nano 6 (2012) 7151–7161, https://doi.org/10.1021/NN302215Y.
[47] A. Terada, A. Yuasa, T. Kushimoto, S. Tsuneda, A. Katakai, M. Tamada, Bacterial adhesion to and viability on positively charged polymer surfaces, Microbiology 152 (2006) 3575–3583, https://doi.org/10.1099/MIC.0.28881-0.
[48] B. Gottenbos, D.W. Grijpma, H.C. van der Mei, J. Feijen, H.J. Busscher, Antimicrobial effects of positively charged surfaces on adhering Gram-positive and Gram-negative bacteria, J. Antimicrob. Chemother. 48 (2001) 7–13, https://doi.org/10.1093/JAC/48.1.7.
[49] B. Gottenbos, H.C. van der Mei, H.J. Busscher, Initial adhesion and surface growth of Staphylococcus epidermidis and Pseudomonas aeruginosa on biomedical polymers, J. Biomed. Mater. Res. 50 (2000) 208–214, https://doi.org/10.1002/(SICI)1097-4636(200005)50:2<208::AID-JBM16>3.0.CO;2-D.
[50] T. Pulingam, K.L. Thong, M.E. Ali, J.N. Appaturi, I.J. Dinshaw, Z.Y. Ong, B.F. Leo, Graphene oxide exhibits differential mechanistic action towards Gram-positive and Gram-negative bacteria, Colloids Surf. B. Biointerf. 181 (2019) 6–15, https://doi.org/10.1016/j.colsurfb.2019.05.023.
[51] A.R. Deokar, L.-Y. Lin, C.-C. Chang, Y.-C. Ling, Single-walled carbon nanotube coated antibacterial paper: preparation and mechanistic study, J. Mater. Chem. B. 1 (2013) 2639–2646, https://doi.org/10.1039/C3TB20188K.
[52] N. Malanovic, K. Lohner, Gram-positive bacterial cell envelopes: The impact on the activity of antimicrobial peptides, Biochim. Biophys. Acta - Biomembr. 1858 (5) (2016) 936–946, https://doi.org/10.1016/j.bbamem.2015.11.004.